SUPPLEMENTARY INFORMATION: SYNTHETIC PLASMONIC LATTICE FORMATION THROUGH INVARIANT FREQUENCY COMBS EXCITATION IN COHERENT GRAPHENE STRUCTURES

Zahra Jalali-Mola¹ and Saeid Asgarnezhad-Zorgabad^{1,*}

¹ Independent Researcher, Personal Research Laboratory, West Ferdows Blvd., Tehran 1483633987, Iran

*sasgarnezhad93@gmail.com

We present the quantitative and qualitative details towards synthetic plasmonic lattice formation in this supplementary information. We start by presenting an example of the nonlinear waveguide, comprising a coherent multi-level atomic medium situated on top of an ultra-low loss double graphene layer. Specifically, we elucidate the specific mechanisms required to excite and probe the system within this design, the multi-level structure, and transitions of the ⁸⁷Rb atoms. We also represent the detailed explanation of scheme feasibility by introducing a realistic source-waveguide-detection triplet in § S.1. Next, we present the detailed quantitative description of our double graphene layer, its optical properties and Ohmic-loss compensation through gain-loss modulation in § S.2. Then, in § S.3 we provide a detailed mathematical steps towards spectral dynamics of the SPP pulse through the hybrid interface and finally in § S.4 we elucidate the additional quantitative steps towards the synthetic plasmonic lattice formation.

S.1. DETAILED DESCRIPTION OF THE WAVEGUIDE CONFIGURATION: AN EXAMPLE WITH MULTI-LEVEL ATOMIC MEDIUM

In this section, we proceed with our approach, by elucidating a specific example of the nonlinear waveguide that meets our conservation conditions, which comprises an atomic ensemble situated on top of the ultra-low loss double-layer graphene. Consequently, first, we present all detailed explanations of the waveguide operation in § S.1 A, and next in § S.1 B, we explain the experimental feasibility for this specific waveguide design. Finally, we discuss the system parameters and challenges of our suggested setup in § S.1 C.

A. Detailed explanation of waveguide operation

To excite invariant PFCs and establish SPL formation, the nonlinear waveguide should possesses suppressed loss and tunable nonlinearity. The dual conditions of loss compensation and tunable nonlinear control can be achieved in an atomic ensemble irradiated with laser fields. The proper injection of laser fields would yield formation of electromagnetically induced transparency windows, for which, the electronic transitions of atomic medium interfere to eliminate or reduce resonant atomic absorption and modulate the linear dispersion. Atomic medium with this spectral transparency windows possesses ultra-low linear absorption and giant nonlinear coefficient. The width related to transparency window nonlinear parameters off this atomic ensemble can be controlled via intensity and detuning of the driven laser fields. Consequently, nonlinear waveguide with double graphene layer as bottom layer and multi-level atomic medium situated on top can be a possible candidate to achieve invariant PFCs and SPL formation. In what follows, we describe the details of the waveguide configuration in details.

To uncover the invariant parameters of NSPPs, we suggest a plasmonic nanostructure as shown in Fig. 1. This waveguide comprises three parts (i) source, (ii) waveguide, and (iii) detection. On one end of the waveguide, a fiber-based connector is attached to couple the source fields to the waveguide, and on the other end, a detection system is connected to detect the output SPP waves. The source fields produce SPPs, plasmonic waveguide controls their spatiotemporal profile that yields linear/nonlinear SPP generation and the detector collects the output intensity of plasmonic fields.

General description- Coherent laser source (CLS) and terahertz generator (THG) are attached to our waveguide using the end-fire coupling technique and irradiate hybrid structure as field sources. THG produces a weak SPP field that is resonant with $|1\rangle \leftrightarrow |3\rangle$ dipole transition [S3] and CLS provides lights that coupled atomic transition as represented in Fig. S1. We employ controllability over intensities and detunings of fields to suppress losses and controlling nonlinearity through the interaction interface. Finally, we detect NSPPs at the output using NSOM technique. In our analysis, we consider a strong couple (c), a signal (s), and a terahertz probe (p) as driving fields that are linearly polarized, possess temporal coherence longer than the waveguide decay, and longitudinally coherent enough to cover the waveguide. The couple and signal laser are obtained through a dye laser and we also control their frequencies through acousto-optic modulators.

On the other hand, our hybrid waveguide comprises a graphene multi-layer as a bottom medium and a cold atomic gas as the upper layer (see Fig. S1). We consider graphene-dielectric-graphene as a multilayer structure that possesses

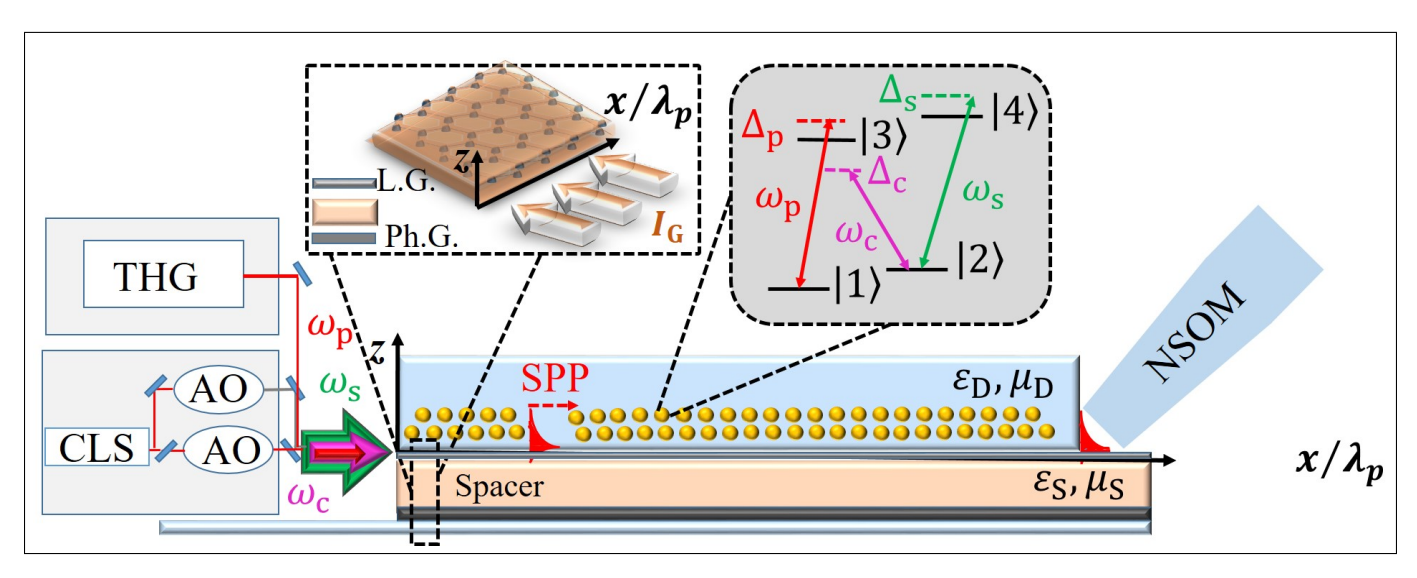


FIG. S1. Source-waveguide-detection triplet to construct an SPL: CLS, and THG irradiate the system and act as *source*. The waveguide comprises cold atomic gas situated on top a double-layer graphene structure. Detection system is attached as an atomic force microscope tip at the end of the waveguide. Right inset represents the atomic medium transitions and the left inset is the double-layer graphene structure design. Detuning frequencies are Δ_l and Rabi frequencies are $\Omega_l \propto E_l$; $l \in \{c, s, p\}$. The inset also shows the atomic states $|j\rangle$ and the details of the coupling mechanism. The symbols are: THG:terahertz generator, CLS: coherent laser source, AO: acousto-optic modulator, L.G: lossy graphene, Ph.G: photo-inverted graphene.

ultra-low loss for our SPP wavelength of interest. Above this structure, an ensemble of 87 Rb cold atoms are situated. Specifically, we consider D line of 87 Rb atoms as four-level N-type atomic medium (4NA) with

$$|1\rangle = |5^2 S_{1/2}, F = 1\rangle, \qquad |2\rangle = |5^2 S_{1/2}, F = 2\rangle,
|3\rangle = |5^2 P_{3/2}, F = 2\rangle, \qquad |4\rangle = |5^2 P_{3/2}, F = 3\rangle,$$
(S1)

as transition levels. Atomic density of this ensemble is $N_{\rm a}$, homogeneous decay rate of the $|m\rangle\leftrightarrow|n\rangle$ transition is γ_{nm} , dephasing rate is $\gamma_{nm}^{\rm deph}$, and the corresponding atomic dipole moment is d_{nm} .

Design of the waveguide- To sum up, our structure is a specific design that includes cold 4NAs and multi-layer

Design of the waveguide- To sum up, our structure is a specific design that includes cold 4NAs and multi-layer graphene structure. 4NAs are appealing due to suppressed absorption commensurate with giant Kerr nonlinearity, thereby this medium provides stable NSPP propagation and FCs generation. On the other hand, we exploit multilayer graphene due to its stable optical properties against the external magnetic field gradient, giant field concentration, and opportunities to provide ultra-low loss plasmonic field propagation. Consequently, our process is coherent, possesses ultra-low loss, and is suitable to provide control over optical nonlinearity. These conditions are necessary to provide suppressed loss and careful nonlinear modification, which are dual requirements for robust PFCs propagation and conservative conditions, and hence our design are the best candidate for SPL formation.

B. Realistic description of the waveguide

In this section, we provide a detailed discussion of the experimental feasibility of our waveguide. As we elucidate in § S.1 A, our waveguide comprises of three parts, namely, (i) source, (ii) waveguide, and (iii) detection. In what follows, we explain the feasible experimental implementation of these parts.

Source- As for sources, two laser fields, a strong couple (c), a signal (s), a terahertz weak probe (p) field, and an additional trigger laser, drive the waveguide. Signal, couple, and probe fields the same polarization and are obtained from an external cavity diode laser that is narrow-band, frequency stabilized, linearly polarized, temporally longer than the waveguide decay, and longitudinally coherent enough to cover the waveguide [S1]. The frequency of the source fields is modified using acousto-optic modulators. Moreover, we propose generating probe field with linear polarization in nanoscopic scale by assuming oxide nanojunctions that is suitable for producing terahertz radiation using ultrafast frequency mixing [S2]. This probe wave will produce the SPP field with a wavenumber ω_p that is in resonance with atomic dipole transition wavelength [S3]. Forth field is a pulsed femtosecond fiber-laser with a few MHz repetition rate, which is linearly polarized, acts as a trigger field, irradiates the plasmonic waveguide from the bottom side and injected perpendicular to the driving laser fields to produce gain for graphene layer [S4]. the

couple and signal fields are injected to the waveguide and co-propagate parallel to the emitter-graphene interface using end-fire coupling technique [S5].

Waveguide- Our waveguide comprises a thin layer atomic medium doped on a lossless dielectric situated on top of a hybrid nanostructure. This plasmonic apparatus comprises two parts. A thin layer foil as a bottom medium that serves as a holder and a double-layer graphene scheme, which is a graphene-spacer-graphene multilayer. This plasmonic scheme should possess low-loss for the dipole transition wavelength. Various methods such as optimization/design, including virtual gain and parametric amplification serve to combat the loss of this plasmonic structure [S6] and hence various ultra-low loss layers can be implemented as our dispersive layer. However, this layer should be robust against magnetic gradient that should be employed for atom cooling.

Graphene structures can be a potential candidate as a metallic-like layer, due to loss tunability and wide spectral bandwidth but producing resonant excitation of NSPPs in optical graphene within a single layer of this structure, unfortunately is challenging due to Ohmic loss and the need for high doping level [S7]. To remedy these limitations, we suggest a double- or multi-layer graphene structures, which is experimentally verified and equivalently act as a single-layer graphene with suppressed dissipation and with high-doping. Our graphene reconfiguration is robust to low magnetic gradients and hence is a suitable candidate for this scheme. We introduce trigger laser to the bottom graphene layer to induce photo-inverted gain [S10] that is exploited to suppresses the Ohmic loss related to this plasmonic structure. Consequently, this configuration would be ultra low-loss for the dipole transition wavelength and we expect stable propagation of linear/nonlinear SPPs within the atomic medium-plasmonic scheme interface.

The interaction interface is filled with a four-level N-type atomic gas (4NA), that is cooled to ultra-low temperatures [S11]. This cold gas serves as electrical dipoles and we also assume the dopant thickness is a few dipole transition wavelengths. 4NAs are appealing due to its efficiency for providing controllable nonlinearity/dispersion and specifically, we consider D line of ⁸⁷Rb atoms with $|1\rangle = |5^2S_{1/2}, F = 1\rangle$, $|2\rangle = |5^2S_{1/2}, F = 2\rangle$, $|3\rangle = |5^2P_{3/2}, F = 2\rangle$ and $|4\rangle = |5^2P_{3/2}, F = 3\rangle$ as transition levels. Atomic density is N_a , homogeneous decay rate of the $|n\rangle \leftrightarrow |m\rangle$ transition is γ_{nm} , dephasing rates are $\gamma_{nm}^{\text{deph}}$ and we neglect the inhomogeneous broadening due to weak Doppler effect. Our laser fields with Rabi frequencies Ω_l and correspond detuning frequencies Δ_l ; $l \in \{c, s, p\}$ drive the atomic medium through dipole approximation. We also assume these fields are tightly confined to the interactive interface with evanescent coupling function $\zeta_l(z)$ [S12].

Detection- The nonlinear plasmonic processes and excited frequency combs are characterized using a detection system. To this aim, a sharpened multimode fiber is attached to the end of the plasmonic waveguide that is called tip, and the plasmonic interface commensurate with tip is illuminated using an infrared focused beam. This field then interacts with NSPPs within the interaction interface, the scattered intensity field profile corresponds to this near-field is then propagates through the tip, the intensity pattern would collects using an image intensifier [S15] and would detect exploiting an atomic force microscope [S3].

Our waveguide reconfiguration is consequently experimentally feasible from source to detection and is efficient to generate controllable linear and Nonlinear SPPs. We achieve the invariant parameters of the NSPPs in three steps. First, we obtain the spatiotemporal and spectral-spatial dynamics of the NSPPs in the presence of nonlinear parameters of the hybrid system. Next, we exploit the quantum properties of nonlinear gain modulation through the hybrid interface and establish a modified nonlinear evolution equation based on invariant parameters of this plasmonic scheme. Finally, we establish the robustness of frequency combs, number of excited plasmon modes, and phase singularity within the interaction interface. Using the robustness of frequency combs, we exploit a synthetic lattice to elucidate the invariant of spectral dynamics and establish the apparition of the anomalous artificial gauge field.

C. Discussion on scheme feasibility

Now, we present the system parameters for which the PFCs serve as invariant of the plasmonic system and can be interpreted as SPL. Then we discuss the challenges and outlook of our suggested scheme.

Scheme feasibility and simulation parameters- First, we test the feasibility of our scheme. We assume $g_{\rm s}=g_{\rm v}=2$, electron Fermi velocity as $v_{\rm F}=10^6$ m/s, chemical potentials for electron (hole) as $\mu_{\rm e}=\mu_{\rm h}=\mu/2\approx0.34$ eV, dielectric constant of spacer as $\varepsilon_{\rm d}=2$, and $d\approx5$ nm. 4NAs are cooled to $T\approx10$ mK using a magneto-optic trap with dB/dz = 10 G/cm and we set $\lambda_{\rm p}=1.55$ eV, $N_{\rm a}=9\times10^{10}$ cm⁻³, $\Omega_{\rm c}\approx30$ MHz, $\Delta_{\rm c}=-2$ MHz, $\Omega_{\rm s}=35$ MHz, $\Delta_{\rm s}=16$ MHz and $\Delta_{\rm p}=0$ and choose relaxation for ⁸⁷Rb from Ref. [S8]. The typical gradient magnetic field to change the optical response of graphene is a few T for a cm interaction length [S9] which is far from gradient field that is needed for magneto-optic trap and hence its effect on NSPP propagation is negligible. With these parameters a SPP with $\mathcal{K}_2=(-4.42+0.4\mathrm{i})\times10^{-12}\mathrm{s}^2\cdot\mathrm{cm}^{-1}$, $W=(2.98+0.6\mathrm{i})\times10^{-11}\mathrm{s}^2\cdot\mathrm{cm}^{-1}$, with group velocity $v_{\rm g}=2\times10^4\mathrm{m/s}$ propagates, we have $g_{\mathcal{K}_2}=1.01$, f=0.045, and $\mathrm{Im}[K_{\rm a}(\omega)]\approx0.06$ cm⁻¹. For gain graphene $\mathrm{Im}[k_{\rm G}]=-0.07$ cm⁻¹,

and for our system $\text{Im}[k_{\text{C}}] = -0.02 \text{ cm}^{-1}$, therefore $\bar{\alpha} = \text{Im}[K_{\text{a}}(\omega) + k_{\text{C}}(\omega)] = 0.04 \approx 0$ that justifies ultra-low loss NSPP propagation.

Our waveguide consequently is suitable for ultra-low loss propagation of NSPPs within the atomic dipole transition wavelength. To simulate SPP propagation in this nonlinear plasmonic system, we assume (i) SPP waves propagate as far plasmonic fields, (ii) the plasmonic phases are constant (i.e. $Kx - \omega t = \text{Const.}$), and (iii) employ mean field-averaging [S12, S13, S14] to consider the evanescent coupling effect. We note that our waveguide for invariant PFCs generation and SPL formation is based on the source-waveguide-detection triplet. The use of coherent laser fields as a source and multi-level atomic layer as the tunable nonlinear medium has two main advantageous, the PFCs excitation process is coherent and the maximum probe laser peak needed to generate NSPPs is very low. Consequently, NSPP generation is efficient and PFCs propagate through the interaction interface for a few tens of nonlinear propagation length.

Finally, we note that our suggested nonlinear waveguide comprises a multi-level atomic medium situated on top of the ultra-low loss plasmonic layer has two challenges. First, the waveguide is a combination of cold atomic medium, double-layer graphene, and coherent laser sources, and its feasibility in a real-life experiment seems a challenge. Consequently, our specific example contains an explicit formalism to achieve invariant PFCs and SPL formation, but its feasibility is challenging and needs further investigation, whose investigation goes beyond the scope of this current work. Second, invariant PFCs and SPL formation is based on justification of the *conservation conditions*, for which a stable propagation of NSPP provides robust PFC excitation. As a detection system of our specific example, we suggest NSOM (near-field scanning optical microscope) technique, due to efficiency for collecting output NSPP fields. The suitability of this technique to establish the conservation condition and the efficiency of NSOM technique to invariant PFC generation looks challenging that need further consideration. We leave the suitable detection technique for uncovering invariant PFCs as a future work.

S.2. LINEAR RESPONSE OF A GRAPHENE LAYER

In this section, we investigate the technical details and mathematical steps towards SPP excitation within our graphene structure. We achieve the loss-compensated plasmonic scheme in three steps: First, we excite the SPP by end-fire coupling of driven laser fields to the graphene-dielectric-graphene multilayer. Next, we suppress the loss related to upper graphene layer by inducing gain to the bottom graphene layer using a photo-inverted scheme introduced in Ref. [S10] for the atomic dipole transition wavelength. The graphene SPP mode for lossy graphene and gain-assisted graphene propagate through this multilayer graphene apparatus. Finally, we couple these two SPP modes using formalism developed in Ref. [S16], to derive the dynamical evolution of the stable graphene SPP mode in the interface between the atomic medium and upper graphene layer.

First, we establish the excitation of SPP wave within graphene layer. This plasmonic field is a TM wave with wavenumber k, frequency ω , phase $\theta = kx - \omega t$, and field profile

$$\boldsymbol{E}(\boldsymbol{r},t) = \boldsymbol{E}(z) \exp\{i\theta\},\tag{S2}$$

$$\boldsymbol{H}(\boldsymbol{r},t) = -\boldsymbol{e}_y H(z) \exp\{i\theta\}. \tag{S3}$$

This field propagates along atomic medium-graphene layer interface whose current density $J = \sigma E$ and surface charge density ρ_{ext} describe by

$$J := J_{s}\delta(z), \tag{S4}$$

$$\rho_{\text{ext}} := \rho_{\text{s}} \delta(z). \tag{S5}$$

The boundary conditions related to this plasmonic system are

$$E_{1t} = E_{2t}, \quad D_{1n} - D_{2n} = \rho_{s},$$
 (S6)

$$B_{1n} = B_{2n}, \quad H_{1t} - H_{2t} = J_s \times n.$$
 (S7)

Now, we replace Eqs. (S2)-(S5) into Maxwell equations, employ the boundary conditions (S6), (S7) to achieve the characteristic dispersion of the SPP wave as

$$\frac{\varepsilon_1}{k_1} + \frac{\varepsilon_2}{k_2} - \frac{4\pi e^2}{k^2} \chi(k, \omega) = 0.$$
 (S8)

for

$$i\omega\chi(k,\omega) = k^2\sigma(k,\omega).$$
 (S9)

Finally we define

$$\tilde{\varepsilon}_{12} := \left(\varepsilon_1^2 - \varepsilon_2^2\right) \left(\varepsilon_1 \mu_2 - \varepsilon_2 \mu_1\right), \quad \tilde{\rho}_s := \frac{\rho_s \omega \varepsilon_1 \varepsilon_2}{C},$$
(S10)

to achieve the propagation constant of the SPP wave

$$k = \left[\frac{(\omega/c)^2 \varepsilon_1 \varepsilon_2 \tilde{\varepsilon}_{12} + 2\tilde{\rho}_s k \varepsilon_1 \varepsilon_2 \sqrt{\tilde{\varepsilon}_{12} + \tilde{\rho}_s^2} + \tilde{\rho}_s^2 (\varepsilon_1^2 + \varepsilon_2^2)}{\varepsilon_1^2 - \varepsilon_2^2} \right]^{1/2},$$
 (S11)

here k_i^z wavevector component is

$$k_j^z = \sqrt{k^2 - \frac{\omega^2 \varepsilon_j \mu_j}{c^2}}, \quad j \in \{1, 2\}.$$
 (S12)

Eq. (S8) with propagation constant (S11) demonstrates the excitation of SPP in our hybrid waveguide [S17].

Next, we represent the SPP wave excitation within our proposed double layer graphene plasmonic waveguide. Our quantitative approach is for characterizing SPP through this interface is based on (i) random phase [S18], and (ii) relaxation time [S19, S10] approximations. Single-graphene layer has valance $\lambda = -$, and conduction $\lambda = +$, bands touching at Dirac points that can be described with chemical potential μ , the interaction interface A, spin (s) and valley (v) degeneracies $g_{\nu} = 2$; $\nu \in \{s, v\}$, and with electron Fermi velocity $v_{\rm F}$ [S20]. Single layer susceptibility within interaction interface that is obtained using random phase approximation

$$\chi(\mathbf{k},\omega) = \frac{g_s g_v}{A} \sum_{q,\lambda,\lambda'=\pm} \frac{n_{q,\lambda} - n_{q+k,\lambda'}}{\hbar\omega + E_{q,\lambda} - E_{q+k,\lambda'} + i0^+} [1 + \lambda\lambda'\cos(\theta_q - \theta_{q+k})], \tag{S13}$$

for \boldsymbol{q} the wave vector, $\theta_{\mathbf{q}}$ the deviation from x-axis, and $E_{q,\lambda} = \lambda \hbar v_{\mathbf{F}} q$ the energy dispersion of electrons with λ and $|\boldsymbol{q}|$. We evaluate (S13) using Fermi distribution function $n_{q,\lambda}$ for near zero temperatures as $n_{q,\lambda} = \Theta(\mu - E_{q,\lambda})$; with μ the chemical potential. We calculate (S13) by employing relaxation approximation (RA) as $\tilde{\omega} = \omega + i\gamma$ to achieve density response for single graphene layer, which includes an undoped part χ^0 and a doped part χ^μ . This doped part characterises the optical properties of the lossy graphene layer for $\mu \neq 0$ through [S18, S21]

$$\chi^{(L)}(k,\tilde{\omega}) = \chi^{(0)}(k,\tilde{\omega}) + \chi^{(\mu)}(k,\tilde{\omega}),\tag{S14}$$

$$\chi^{(0)}(k,\tilde{\omega}) = \frac{-ig_{\rm s}g_{\rm v}k}{16\hbar\sqrt{\tilde{\omega}^2 - v_{\rm F}^2k^2}}, \quad \chi^{\mu}(k,\tilde{\omega}) = \frac{g_{\rm s}g_{\rm v}\mu}{8\pi\hbar^2v_{\rm F}^2} \left[-4 + \left(\frac{\hbar v_{\rm F}k}{\mu}\right)^2 \frac{G(x^+) + G(x^-)}{2\sqrt{\tilde{\omega}^2 - v_{\rm F}^2k^2}} \right], \tag{S15}$$

for

$$G^{\pm}(x) = x\sqrt{x^2 - 1} - \ln\left(x + \sqrt{x^2 - 1}\right), \quad x^{\pm} = \frac{\hbar\tilde{\omega} \pm 2\mu}{\hbar v_{\rm F} k},$$
 (S16)

and we take into account the collision loss as a relaxation to perturbation frequency by employ mapping

$$\omega \mapsto \tilde{\omega} = \omega + i\gamma, \tag{S17}$$

for $\gamma = \tau^{-1}$ the electric relaxation frequency [S10]. Eq. (S15) commensurate with (S17) describes the spectral evolution of the lossy graphene. Next, we couple a trigger field $I_{\rm G}$ to modulate electron (hole) chemical potential $\mu_{\rm e}$ ($\mu_{\rm h}$) for a gain-assisted graphene medium, and obtain corresponding density response function through mapping

$$\chi^{(\mu)}(k,\tilde{\omega}) \mapsto \chi^{(\mu_{\rm e})}(k,\tilde{\omega}) + \chi^{(\mu_{\rm h})}(k,\tilde{\omega}).$$
 (S18)

Next we exploit (S15) to achieve [S10]

$$\chi^{(G)}(k,\tilde{\omega}) = \chi^{(0)}(k,\tilde{\omega}) + \chi^{(\mu_e)}(k,\tilde{\omega}) + \chi^{(\mu_h)}(k,\tilde{\omega}). \tag{S19}$$

Eqs. (S15) and (S19) justify SPP propagation in our hybrid plasmonic system.

Finally, we investigate the coupling between these gain-loss doublet in our configuration. To this aim, we assume a dielectric spacer between gain-loss paired graphene layers ε_d , neglect the orbital overlap and employ Coulomb interaction to achieve the effective susceptibility of the coupled layer as χ^C , and evaluate the hybrid plasmonic system dielectric function as

$$\varepsilon(k,\omega) = \mathbf{1} - \boldsymbol{\chi}^{(C)}(k,\omega)\boldsymbol{V}(k),$$
 (S20)

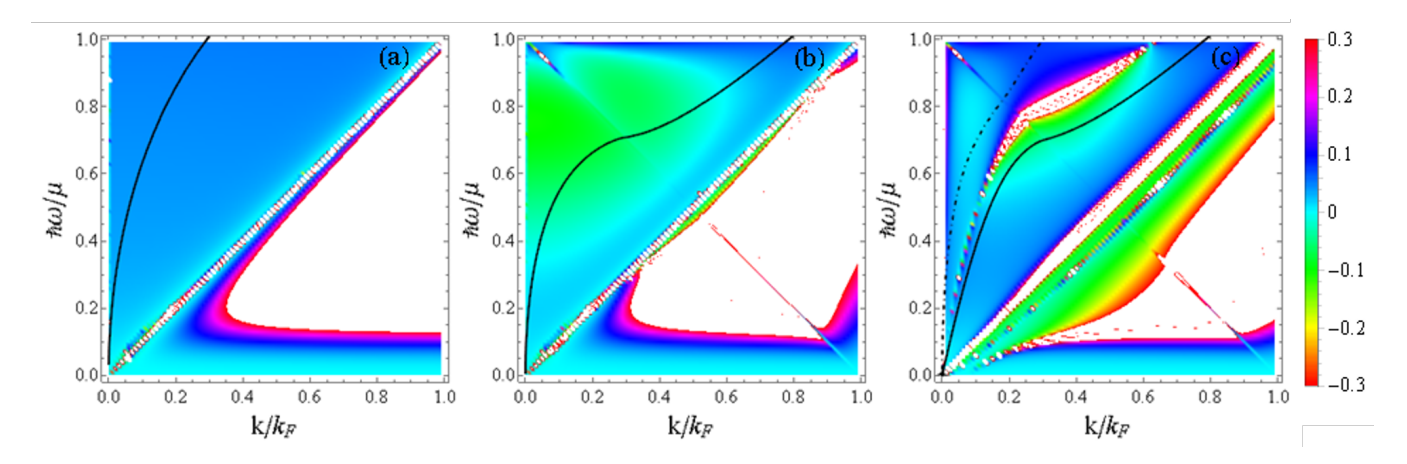


FIG. S2. Spectral evolution of the graphene SPP within hybrid interface as a function of normalized energy $\hbar\omega/\mu$ and normalized momentum $k/k_{\rm F}$: Panel (a) represent the SPP dispersion for lossy graphene, panel (b) depicts the SPP in a hybrid interface with gain assisted graphene and panel (c) shows the SPP behavior in coupled gain-loss graphene bi-layer. Parameters used for these simulations are: $\epsilon_1 = \epsilon_2 = 1$, $g_{\rm s} = g_{\rm v} = 2$, $c = 3 \times 10^8$ m/s and $v_{\rm F} = 10^6$ m/s, $\hbar\tau^{-1}/\mu = 0.08$ Hz [S10]. For panel (c) $\epsilon_{\rm d} \approx 2$ and $k_{\rm F}d = 4.43$ [S24]. Normalized waveguide decay is characterized by $\hbar\gamma/\mu$ as a color bar. See text for detailed explanation.

in which potential matrix is characterized by diagonal intra-layer $V_{11} = V_{22}$ and off-diagonal inter-layer $V_{12} = V_{21}$ elements [S22]

$$V_{ij} = \frac{8\pi e^2}{kD} \varepsilon_{\rm d},\tag{S21}$$

$$V_{ii} = \frac{4\pi e^2}{kD} \left[(\varepsilon_d + \varepsilon_1) \exp\{kd\} + (\varepsilon_d - \varepsilon_2) \exp\{-kd\} \right], \tag{S22}$$

with [S23]

$$D = (\varepsilon_1 + \varepsilon_d)(\varepsilon_d + \varepsilon_2) \exp\{kd\} + (\varepsilon_1 - \varepsilon_d)(\varepsilon_d - \varepsilon_2) \exp\{-kd\}.$$
 (S23)

In our analysis, we assume the density response of the coupled gain-loss system $\chi^{(C)}(k,\tilde{\omega})$ as a diagonal matrix (i.e. with $\chi_{ij}^{(C)}(k,\tilde{\omega})=0$). Each diagonal element of which represents the corresponding density response of each layer in coupled gain-loss system. Plugging Eq. (S22) into (S20) would yield the characteristic equation for SPP dispersion [S24, S25]

$$\left[1 - V_{11}(k)\chi_{11}^{(C)}(k,\omega)\right] \left[1 - V_{22}(k)\chi_{22}^{(C)}(k,\omega)\right] - V_{12}(k)V_{21}(k)\chi_{11}^{(C)}(k,\omega)\chi_{22}^{(C)}(k,\omega) = 0, \tag{S24}$$

which establishes excitation of stable SPP mode for coupled gain-loss graphene layers.

We represent the spectral evolution of the excited SPPs for single lossy graphene, gain assisted graphene and gainloss paired double graphene layers in Fig. S2. The SPP within Pauli-blocked inter-band characterized by $\hbar(\omega + v_F k) < 2\mu$ and $\omega > v_F k$ would be dissipative along graphene-dielectric interface due to relaxation decays as clearly shown in Fig. S2(a). For a gain assisted graphene, however, we couple a trigger laser to induce population inversion between valance and conduction band, hence the gain is provided for effective zero carrier density $\mu_h = \mu_e = \mu/2$ [S10]. This laser-induced mechanism yields modification in graphene density response, suppresses the loss due to additional gain induction and consequently results in loss-free propagation of graphene SPP as we establish in Fig. S2(b). Finally, in a gain-loss paired graphene double layers separated by a spacer, two-mode graphene SPP propagation is expected due to coupled-mode theory [S24], which are propagated along the hybrid interface and characterized by dashed-dotted and solid lines in Fig. S2(c). We consider the dynamical evolution of the solid line SPP mode due to gain-assisted loss compensation. The dashed-dotted line SPP mode is highly dissipative and consequently its propagation length is highly limited due to total loss of graphene layer.

We test the feasibility of loss-free SPP mode propagation along gain-loss paired double-layers by choosing the realistic parameters. The carrier density is [S26]

$$n_{\rm s} = \frac{g_{\rm s}g_{\rm v}\mu^2}{4\pi\hbar^2 v_{\rm F}^2} \approx 10^{11} \text{ cm}^{-2},$$
 (S25)

and the Fermi surface momentum is $k_{\rm F}=10^9{\rm m}^{-1}$. Considering the degeneracies as $g_{\nu}=2$, and $v_{\rm F}=c/300$, the low-loss propagation of the SPP within this coupled plasmonic scheme would be excited for our dipole transition wavelength $\lambda=800$ nm and $k/k_{\rm F}\approx0.5$ [S20], which establishes our assumptions within Fig. S2(c). Consequently, this SPP mode interacts with the nonlinearity and dispersion of the interface and possess spatiotemporal evolution.

S.3. SPECTRAL EVOLUTION OF THE PLASMONIC FREQUENCY COMBS IN THE PRESENCE OF INVARIANTS

In this section, we provide the main steps towards the mathematical details of the derivation of the Eq. (8). We present our quantitative approach in two subsections. First in § S.3 A, we use a classical treatment and employ nonlinear modification to establish the existence of system invariant through our nonlinear dissipative interface. Next, in § S.3 B we employ the quantum theory of soliton [S33] and employ mean-value quantum field evolution to achieve the spectral field dynamics of the plasmonic frequency combs in the presence of conserved energy and conserved number of excited SPP modes, thereby derive Eq. (8) of the main text.

A. Existence of system conservatives and derivation of Eq. (6)

We represent the qualitative approach towards system conservatives in two sub-sections. First, we evaluate the dynamical evolution of the nonlinear SPP field within our interaction interface and derive Eq. (3) of the main text. Next, we introduce energy and number of excited SPP mode as the two nonlinear parameters that affect the dynamics of frequency combs and establish the conservations of these quantities through nonlinear interaction, thereby present detailed derivation of Eq. (6).

1. Nonlinear SPP field dynamics and derivation of Eq. (3)

Our starting point is the propagation of the field within the nonlinear interface

$$\nabla \times \nabla \times \boldsymbol{E} + \frac{1}{c^2} \frac{\partial^2 \boldsymbol{D}}{\partial t^2} = -\frac{1}{\varepsilon_0 c^2} \frac{\partial^2 \boldsymbol{P}}{\partial t^2},$$
 (S26)

for

$$\boldsymbol{D}(\boldsymbol{r},t) = \int_0^{t_S} dt' \varepsilon(t') \boldsymbol{E}(\boldsymbol{r},t-t'), \tag{S27}$$

$$P(\mathbf{r},t) = E(\mathbf{r},t) \int_0^{t_S} dt' \chi^{(3)}(\mathbf{r},t') |E(\mathbf{r},t-t')|^2,$$
 (S28)

the displacement vector and nonlinear polarization, respectively and for $\varepsilon(t')$, $\chi^{(3)}(t')$ the susceptibility and Kerr nonlinear coefficient of the interaction interface. In the Fourier space, we represent the electric field as $\Psi(\mathbf{r},\omega)$ with

$$\Psi(\mathbf{r},\omega) := F(\mathbf{r},\omega)\tilde{A}(x,\omega),\tag{S29}$$

 $F(r,\omega)$ the spectral-spatial mode distribution in the interaction interface, $\tilde{A}(x,\omega)$ the field distribution along interaction direction and $\mathcal{K}(\tilde{\omega})$ the dispersion of the plasmonic field. We assume the Fourier transform of the probe field as

$$E(\mathbf{r},t) = \int d\omega \Psi(\mathbf{r},\omega) \exp\{i\mathcal{K}(\omega)x - i\omega t\}.$$
 (S30)

We exploit Eq. (S30) to evaluate temporal dynamics of the displacement vector and nonlinear polarization as

$$\frac{\partial^2 \mathbf{D}}{\partial t^2} = -\int d\omega \left[\omega^2 \varepsilon(\mathbf{r}, \omega) F(\mathbf{r}, \omega) \tilde{A}(x, \omega) \exp\{i\mathcal{K}x\} \right], \tag{S31}$$

$$\frac{\partial^{2} \mathbf{P}}{\partial t^{2}} = -\int d\omega \left[\omega^{2} \iint d\omega' d\nu \exp\{i\Delta \mathcal{K}x\} \chi_{\omega-\nu}^{(3)}(\mathbf{r}) \tilde{A}_{\omega-\nu+\omega'}(x) F_{\omega-\nu+\omega'}(r) \tilde{A}_{\nu}^{*}(x) F_{\nu}^{*}(r) \tilde{A}_{\omega'}(x) F_{\omega'}(r) \right], \quad (S32)$$

with

$$\Delta \mathcal{K} = \mathcal{K}(\omega - \nu + \omega') - \mathcal{K}(\nu) + \mathcal{K}(\omega') - \mathcal{K}(\omega), \tag{S33}$$

and we also ignore the spatial distribution of the optical Kerr nonlinearity $\chi_{\omega-\nu}^{(3)}(r) \approx \chi^{(3)}(\omega-\nu)$. Next, we substitute Eqs. (S31) and (S32) into Eq. (S26) and exploit

$$\mathcal{K}^2 = \frac{\varepsilon^2(\mathbf{r}, \omega)\omega^2}{c^2} \tag{S34}$$

to achieve

$$\mathbf{E}(x,\omega)\nabla_{\perp}^{2}F(\mathbf{r},\omega) + F(\mathbf{r},\omega)\left[2\mathrm{i}\mathcal{K}(\omega)\frac{\partial}{\partial x} + \frac{\partial^{2}}{\partial x^{2}}\right]\mathbf{E}(\mathbf{r},t) = -\frac{\omega^{2}}{\varepsilon_{0}^{2}c^{2}}\iint d\omega'd\nu \exp\{\mathrm{i}\Delta\mathcal{K}x\}\chi_{\omega-\nu}^{(3)}(\mathbf{r})\tilde{A}_{\omega-\nu+\omega'}(x)F_{\omega-\nu+\omega'}(r)\tilde{A}_{\nu}^{*}(x)F_{\nu}^{*}(r)\tilde{A}_{\omega'}(x)F_{\omega'}(r).$$
(S35)

In this work we employ slowly varying amplitude approximation (i.e. $\partial^2/\partial x^2 \mapsto 0$). We then multiple both sides of Eq. (S35) by $F(\mathbf{r},\omega)$ and perform integration over all possible transverse coordinates. Using

$$E(x,\omega)\int d\mathbf{r}F(\mathbf{r},\omega)\nabla^2 F(\mathbf{r},\omega) = 0,$$
 (S36)

define the Green's function of the medium as

$$G(\omega, \omega', \nu) := \frac{\int d\mathbf{r} F_{\omega}(r) F_{\omega'}(r) F_{\nu}^*(r) F_{\omega - \nu + \omega'}(r)}{\int d\mathbf{r} F_{\omega}^2(r)},$$
(S37)

and effective refractive index of the medium as

$$n_{\text{eff}}(\omega) = \frac{c\mathcal{K}(\omega)}{\omega} \tag{S38}$$

we achieve the spectral evolution of the field in the interaction interface as

$$\frac{\partial \Psi(\omega, x)}{\partial x} = \frac{2i\pi\omega}{n_{\text{eff}}(\omega)c} \iint d\omega' d\nu \chi^{(3)}(\omega - \nu) G(\omega, \omega', \nu) \tilde{A}_{\omega'}(x) \tilde{A}_{\omega}^*(x) \tilde{A}_{\omega-\nu+\omega'}(x). \tag{S39}$$

In this work, we neglect the field variation along longitudinal direction y and we assume the field is concentrate at interface through the transverse direction as $|E(z)| \sim \exp\{-\text{Im}[\mathcal{K}(\omega)]z\}$. We assume this coupling coefficient as $\zeta(z)$. Our predicted nonlinear field propagation, therefore, is valid for effective propagation length L_{eff} and interaction interface S_{eff} that can be evaluated using the transverse distribution and Eq. (S37) as

$$L_{\text{eff}} = \frac{1}{\alpha_{\text{eff}}} \left[1 - \exp\{-a_{\text{eff}} x_{\text{max}}\} \right],$$
 (S40)

$$S_{\text{eff}} = \frac{\left(\int_{-\infty}^{+\infty} \int_{-\infty}^{+\infty} dx dz \left| \zeta(z) F(y, z; \omega') \right|^2 \right)^2}{\int_{-\infty}^{+\infty} \int_{-\infty}^{+\infty} dx dz \left| \zeta(z) F(y, z; \omega') \right|^4}.$$
 (S41)

Now we define the coefficient characterizing the self-phase modulation $\mathcal{W}(\omega)$ as

$$W(\omega') := \frac{n_2(\omega')}{cS_{\text{eff}}}.$$
 (S42)

In our analysis, the hybrid interface possesses ultra-low Ohmic loss only for the small deviation of the SPP field frequency. as a result, consiedring the small frequency perturbation as $\omega' = \omega + \omega_{\text{SPP}}$, the self-phase modulation can be expanded as a Tylor series

$$W(\omega) = W_0 + W_1 \delta \omega + W_2 \delta \omega^2 + \mathcal{O}(\delta \omega^3). \tag{S43}$$

Our predicted nonlinear plasmonic effects are valid for certain coherence timescale that we evaluate by plugging Eq. (S43) to Eq. (S42) and truncate the Taylor expansion only to first order. The specific nonlinear timescale then is

$$t_{\rm S} = \tau_0 + \frac{\mathrm{d}}{\mathrm{d}\omega} \left[\ln \left(\frac{1}{n_{\rm eff} S_{\rm eff}} \right) \right]_{\omega = \omega_{\rm SPP}},$$
 (S44)

that is defined as the characteristic time-length for which the nonlinear interaction of the system can be described by the nonlinearity modulated as Eq. (S43).

For the modulated SPP field characterised as Eq. (S29), we achieve the propagation constant as $\mathcal{K}(\omega) := \beta(\omega) + k(\omega)$; $\beta(\omega)$ is the linear chromatic dispersion of the atomic medium and $k(\omega)$ given by Eq. (S29). Consequently, we include this dispersion into the spectral evolution of the SPP field to achieve

$$\frac{\partial \Psi(\omega, x)}{\partial x} = i\mathcal{K}(\omega)\tilde{A}(x, \omega) + \frac{2i\pi\omega}{n_{\text{eff}}(\omega)c} \iint d\omega' d\nu \chi^{(3)}(\omega - \nu)G(\omega, \omega', \nu)\tilde{A}_{\omega'}(x)\tilde{A}_{\nu}^*(x)\tilde{A}_{\omega-\nu+\omega'}(x). \tag{S45}$$

Eq. (S45) contains a nonlinear term that acts as a convolution that connects the amplitudes of the SPP field with different amplitudes. This term hence characterizes the nonlinear interaction through the interface. In this work, we aim to investigate the plasmonic frequency combs, which connects the three nearest neighbor frequencies $\omega - \omega_m$, ω and $\omega + \omega_m$ and we assume the frequency combs are equally distanced and descritized. Therefore the frequency indices in Eq. (S45) should change to ω , $\omega \pm \omega_m$, respectively and we also consider mapping $\int d\nu \mapsto \sum_m$ to includes all the stable frequency combs. Then we achieve

$$i\frac{\partial \tilde{\Psi}(\boldsymbol{r},\omega)}{\partial x} = \mathcal{K}(\omega)\tilde{\Psi} + \iint d\nu d\omega' \frac{\mathcal{W}^{0}(\omega')}{(2\pi)^{2}} \tilde{\Psi}^{*}_{\omega'-\nu}(\boldsymbol{r},\omega')\tilde{\Psi}_{\omega'}(\boldsymbol{r},\varpi)\tilde{\Psi}_{\omega'+\nu}(\boldsymbol{r},\nu)e^{i\Delta\mathcal{K}x}, \tag{S46}$$

that is Eq. (3) of the main text.

2. Existence of conservation and nonlinear plasmonic field modulation

In this section, we elucidate our quantitative description towards existence of conserved parameters and then modulate the nonlinearity for simultaneous conservation of energy and number of excited SPP mode. We notice that the frequency combs then excite due to nonlinearity and dispersion management similar to Ref. [S28]. These plasmonic combs would possess ultra-low loss of the frequencies within electromagnetically induced transparency windows of the atomic medium due to suppressed dissipation. In this interface with modulated nonlinearity characterized by Eq. (S43) these combs take the form

$$\Psi(\mathbf{r},t) \sim \sum_{m=1}^{N_{\text{EIT}}} A_m(x) \exp\{i\omega_m t\},\tag{S47}$$

the total energy of the excited SPP frequency combs are

$$E \propto \sum_{m=1}^{N_{\text{EIT}}} |A_m(x)|^2, \qquad (S48)$$

and we take the number of excited frequency combs as

$$\mathcal{N} \propto \sum_{m=1}^{N_{\text{EIT}}} \frac{|A_m(x)|^2}{\omega_{\text{SPP}} + \omega_m}.$$
 (S49)

We then take derivative with respect to x from both side of Eqs. (S48) and (S49) and evaluate the spatial variation of the energy $\partial E/\partial x$ and number of excited frequency combs $\partial \mathcal{N}/\partial x$ as

$$\frac{\partial E}{\partial x} \propto -\bar{\alpha} \sum_{m} |A_m(x, \tilde{\omega})|^2 + \sum_{m} [\mathcal{W}(\omega_{\rm ch}) + \mathcal{W}(\omega_0) - \mathcal{W}(\omega_-) - \mathcal{W}(\omega_+)] \Delta, \tag{S50}$$

$$\frac{\partial \mathcal{N}}{\partial x} \propto -\bar{\alpha} \sum_{m} \frac{|A_m(x,\tilde{\omega})|^2}{\omega_0 + \omega_m} + \sum_{m} \left[\frac{\mathcal{W}(\omega_0)}{2\omega_0} + \frac{\mathcal{W}(\omega_-)}{\omega_0 + \omega_-} + \frac{\mathcal{W}(\omega_+)}{\omega_0 + \omega_+} \right] \Delta, \tag{S51}$$

for $W(\omega_{\rm ch})/(\omega + \omega_{\rm ch}) \approx 0$. In writing Eqs. (S50) and (S51) we assume

$$\Delta := 4\operatorname{Im}\left[A_1^* A_2 A_3 A_4^* \exp\{i\Delta \mathcal{K}_t x\}\right] \tag{S52}$$

as the detuning of the SPP fields through four-wave mixing process with

$$\Delta \mathcal{K}_{t} = \mathcal{K}(\omega_{ch}) + \mathcal{K}(\omega_{+}) - \mathcal{K}(\omega_{0}) - \mathcal{K}_{4}(\omega_{-}), \tag{S53}$$

denotes the phase mismatch between the different SPP field and

$$\mathcal{K}(\omega_l) = \beta(\omega_l) + k(\omega_l) + \sum_{n=1}^{\prime} \sum_{l=1}^{n} (2 - \delta_{ln}) \mathcal{W}(\omega_l) |A_n(\omega_l)|^2,$$
 (S54)

for $n \in \{+, -, 0, \text{ch}\}$, represent the nonlinear wavenumber of the plasmonic interface. Also, the prime in Eq. (S54) denotes that the summation performed over all possible frequency combs.

It is obvious from Eq. (S50) that by modulating $W(\omega) = W_0 + W_1 \omega$ the energy becomes invariance of the system but the number of excited frequency combs would be varying. On the other hand, by choosing $W(\omega) = W'_1(\omega + \omega_{\text{SPP}}) + W'_2(\omega + \omega_{\text{SPP}})^2$, the number of modes become the invariant off the system, but we loose the energy conservation. However, the simultaneous invariant for both energy and number of excited SPP waves is achieved through nonlinearity modulation as

$$W = W_0 + \left(\frac{W_0}{\omega_{\text{SPP}}}\right)\omega,\tag{S55}$$

that is Eq. (5) of the main text for $\omega_{\text{SPP}} \mapsto \omega_0$. As it is clear from Eq. (S55), energy and number of excited SPP modes would become conserved parameter of the system if we linearize the nonlinearity as this equation and also perturb the frequency only for $\tilde{\omega} = \omega + \omega_{\text{SPP}}$. We refer these two conditions as the conservation conditions for the plasmonic system.

B. Mean-field evolution of quantum nonlinear SPP mode and derivation of Eq. (6)

In this section we elucidate our quantitative approach for the derivation of Eq. Eq. (6) of the main text. We notice that our conservative parameters do not depend on the dispersion of the system, then we can set $\mathcal{K}(\omega) = 0$ To obtain this equation, we use the quantum theory approach of optical soliton within a nonlinear fiber [S33] and extend it to our dissipative hybrid nonlinear interface. Similar to Ref. [S33], we assume that our nonlinear Schrödinger equation can also be derived through mean-value evolution of the quantum SPP field operator through Schödinger equation

$$\frac{\partial}{\partial x} |\psi\rangle = H_{\rm I} |\psi\rangle. \tag{S56}$$

We introduce $|\psi\rangle$ as the quantum state of light, and

$$\mathcal{H}_{\rm I} = \sum_{m} \iint d\tilde{\omega} d\omega \frac{\mathcal{W}^{0}}{2} \hat{\boldsymbol{b}}_{\omega}^{\dagger} \hat{\boldsymbol{b}}_{\tilde{\omega}}^{\dagger} \hat{\boldsymbol{b}}_{\tilde{\omega} - \omega_{m}} \hat{\boldsymbol{b}}_{\tilde{\omega} + \omega_{m}}. \tag{S57}$$

as the nonlinear interaction Hamiltonian of the SPP field.

Here we assume the most general case for which $\hat{\boldsymbol{b}}_{j}(\boldsymbol{r},\omega)$ ($\hat{\boldsymbol{b}}_{j}^{\dagger}(\boldsymbol{r},\omega)$); $j \in \{\text{e, m}\}$ as annihilation (creation) operators associated with the electrical (e) and magnetic (m) response of the medium, whose components are described by usual bosonic commutation relation

$$\left[\hat{b}_{ji}(\mathbf{r},\omega),\hat{b}_{j'j}(\mathbf{r}',\omega')\right] = 0, \tag{S58}$$

$$\left[\hat{b}_{ji}(\mathbf{r},\omega),\hat{b}_{j'j}^{\dagger}(\mathbf{r}',\omega')\right] = \delta_{ij}\delta_{jj'}\delta(\omega-\omega')\delta(\mathbf{r}-\mathbf{r}'). \tag{S59}$$

 \mathcal{W}^0 contains the frequency dependent, but we assume the frequencies are all exist within the stable NSPP frequency range. In this case, Eq. (S57) yields stable multiple plasmonic four-wave mixing. As in § S.3 A to consider the energy and number of excited frequency combs as conservatives of the system, we employ mapping $\omega \mapsto \omega_m + \omega_{\text{SPP}}$, and assume $\mathcal{W}^0 = \mathcal{W}^{0*}$. The quantum SPP field within the interaction interface takes the form

$$\Psi(\mathbf{r},t) = \int_{\mathbf{r}',\tilde{\omega}} \hbar\tilde{\omega} \left[\mathbf{A}(\mathbf{r},\mathbf{r}';\tilde{\omega}) \cdot \hat{\mathbf{j}}(\mathbf{r}',\tilde{\omega}) e^{i\tilde{\omega}t} + h.c \right].$$
 (S60)

for $\mathcal{A}(r, r'; \tilde{\omega})$ the green function of the interface [S29],

$$\hat{\boldsymbol{j}}(\boldsymbol{r},\omega) = -2\pi i \omega \alpha(\boldsymbol{r},\omega) \hat{\boldsymbol{b}}_{e}(\boldsymbol{r},\omega), \tag{S61}$$

the quantized current density of the graphene interface and with

$$\alpha(\mathbf{r},\omega) = \left\{ \frac{\hbar \varepsilon_0}{\pi} \text{Im}[\varepsilon(\mathbf{r},\omega)] \right\}^{1/2}, \tag{S62}$$

the constant of the system depends on the medium. Plugging Eqs. (S61) and (S62) into Eq. (S60) and making use of (S29), we see that the quantized plasmonic frequency combs \hat{A}_m are

$$\hat{A}_m(\mathbf{r},\omega) \propto \sqrt{\frac{\hbar\omega}{\varepsilon_0 V}} \hat{\mathbf{b}}(\mathbf{r},\omega) + \text{c.c.}.$$
 (S63)

Next, we substitute the necessary condition for energy and number of SPP mode conservation (i.e. $\omega \mapsto \omega_m + \omega_{\rm SPP}$) and substitute into Eq. (S56) we achieve the mean value evolution of the stable plasmonic frequency combs in the presence of the conservatives of the system as

$$\frac{\partial \langle \hat{A}_m \rangle}{\partial x} = i \iint d\tilde{\omega} d\omega \Lambda(\omega, \tilde{\omega}, \omega_m) \hat{\boldsymbol{b}}_{\omega}^{\dagger} \hat{\boldsymbol{b}}_{\tilde{\omega}}^{\dagger} \hat{\boldsymbol{b}}_{\tilde{\omega} - \omega_m} \hat{\boldsymbol{b}}_{\tilde{\omega} + \omega_m}.$$
 (S64)

 Λ the nonlinearity of four-wave mixing process for frequency around $\omega_{\rm SPP}$, which we define as

$$\Lambda \propto \left\langle \frac{(\mathcal{W}_{\omega,\tilde{\omega},\omega-\omega_{m},\tilde{\omega}+\omega_{m}}^{0} + \mathcal{W}_{\tilde{\omega},\omega,\tilde{\omega}+\omega_{m},\omega-\omega_{m}}^{0})\sqrt{\hbar(\omega+\omega_{\mathrm{SPP}})/\varepsilon_{0}V}}{2\sqrt{(\omega_{\mathrm{SPP}}+\omega-\omega_{m})(\omega_{\mathrm{SPP}}+\tilde{\omega}+\omega_{m})(\omega_{\mathrm{SPP}}+\tilde{\omega})}} \right\rangle_{z},$$
(S65)

and we consider the SPP field properties as evanescence coupling and employ field-averaging as in Ref. [S12].

Eq. (S65) is obtained from mean-field evolution of the quantum plasmonic frequency combs in the presence of the SPP field dispersion and dissipation and represents the nonlinearity, which is obtained in the presence of energy and number of excited SPP modes conservation. Due to quantum theory of soliton [S33], we expect the nonlinearity is equivalent to the nonlinearity obtained in NLSE. Therefore, in order to modulates the nonlinearity to include conservatives to NLSE, we employ mapping $\Lambda \mapsto W$ in Eq. (S46). Next, we include the dispersion of the system as $\mathcal{K}(\omega)$. Finally we define

$$\iint d\omega d\tilde{\omega} \mapsto \mathcal{F} \tag{S66}$$

as Fourier transform operator. In this case by substituting into Eq. (S64) we achieve

$$\frac{\partial \tilde{A}}{\partial x} = i\mathcal{K}(\omega)\tilde{A} + \sum_{m} \mathcal{F}\left[\Lambda(\tilde{\omega})|A_{m}|^{2}A_{m}\right] + \text{c.c.}, \tag{S67}$$

which is the Eq. (6) of the main text. This equation is the same as nonlinear Schödinger equation, as it includes the nonlinear parameters of the system, however this equation differs trivial nonlinear Schrödinger equation as we introduce the energy and number of excited SPP modes as the conservatives of the system.

S.4. CONSTRUCTION OF PLASMONIC SYNTHETIC LATTICE

In this section we present the detailed steps towards synthetic lattice formation within our hybrid nonlinear plasmonic interface. Our quantitative method for constructing the synthetic lattice is based on two steps. First, we explore the NSPP dynamics and excitation of the NSPPs within hybrid interface in § S.4 A, and next, we elucidate the main steps towards mapping to a synthetic lattice in § S.4 B. It is worth noting to indicate that the formation of this synthetic lattice is crucially depend on the existence of invariants of the NSPPs. Formation of the synthetic lattice corresponds to lossy NSPPs needs further consideration and can be considered as a future work.

A. Formation of NSPP and generating frequency combs through interaction interface

In this section, we elucidate the main steps towards NSPPs excitation in normalized length ($\xi := x/L_{\rm NL}$) and normalized time ($\varrho := \tau/\tau_0$) and then establish the existence of surface polaritonic frequency combs. The dynamical evolution of a normalized SPP field ($u(\xi,\varrho) := \Omega_{\rm p}(\xi,\varrho)/U_0$) in the interface between a nonlinear medium, and a metallic-like interface, whose nonlinear parameters are characterized by self-phase modulation (W) and group-velocity dispersion (K_2), is described by nonlinear Schrödinger equation [S12, S28]

$$i\frac{\partial u(\xi,\varrho)}{\partial \xi} + \frac{1}{2}K_2\frac{\partial^2 u(\xi,\varrho)}{\partial \varrho^2} + W|u(\xi,\varrho)|^2 u(\xi,\varrho) = 0.$$
 (S68)

Similar to other nonlinear systems, Eq. (S68) possesses exact solutions that are known as peregrine waves $u_{\text{Pe}}(\xi, \varrho)$ and Akhemediev breather $u_{\text{AB}}(\xi, \varrho)$ [S30]. Next, we employ a Fourier transform of these exact solutions

$$A_m(\xi, \tilde{\omega}) = \frac{1}{\sqrt{2\pi}} \int_0^\infty d\varrho u_l(\xi, \varrho) \exp\{i\tilde{\omega}_m \varrho\}, \quad l \in \{\text{Pe, AB}\},$$
 (S69)

and evaluate the integral to obtain the spectral harmonic side-band amplitudes $A_m(\xi)$ for $\tilde{\omega} = \omega \pm m\Omega/2$; $m \in \{\pm 2, \pm 4, \ldots\}$ and we define $\Omega := \omega_{\rm EIT}/\mathcal{N}$ as frequency spacing. In our plasmonic interface, we achieve the harmonic side-bands amplitudes correspond to resonant mode A_0 as and other frequency side-band as

$$A_0(\xi) = 1 - \frac{ib \sinh\{b\xi\} + p^2 \cosh\{b\xi\}}{\sqrt{\cosh^2\{b\xi\}} - 2a},$$
(S70)

and higher-order spectral side-band as

$$A_m(\xi) = \frac{ib \sinh\{b\xi\} + p^2 \cosh\{b\xi\}}{\sqrt{\cosh^2\{b\xi\}} - 2a} \left[1 - \frac{\cosh\{b\xi\}\sqrt{\cosh^2\{b\xi\}} - 2a}{\sqrt{2a}} \right]^{|m|}.$$
 (S71)

Here, we assume P_0 as the input power of the SPP field, and also consider ω as the modulation frequency off the SPP field. Also, we define

$$\omega_{\mathcal{C}} = \sqrt{\frac{4\gamma P_0}{|K_2|}},\tag{S72}$$

as the characteristic frequency of the system. Then we achieve the modulation parameters a, b in terms of these quantities as

$$2a = \sqrt{1 - \left(\frac{\omega}{\omega_c}\right)^2}, \quad b = \sqrt{8a(1 - 2a)}, \tag{S73}$$

In the limiting case $a \mapsto 0.5$ SPP will propagated as plasmonic peregrine wave and we find the spectral harmonic side-band amplitudes by employing harmonic $a \mapsto 0.5$ to Eqs. (S70), (S71).

The spatial-spectral evolution of these harmonic side-bands are represented in Fig. S3(a). Consequently, generation of NSPPs within a nonlinear hybrid plasmonic interface would yield the excitation of harmonic side-bands with characteristic frequency ω_m and amplitude $A_m(\xi)$ that are propagated along the interaction interface up to a few nonlinear propagation length.

B. Synthetic lattice formation based on NSPP parameters

In this section we elucidate the necessary steps towards synthetic lattice formation of propagated frequency combs. To this aim, first we describe the general properties of the synthetic lattice and describe the sites and hopping related to this system, and next we explain the synthetic lattice Hamiltonian and elucidate the evolution of the synthetic structure in terms of system parameters.

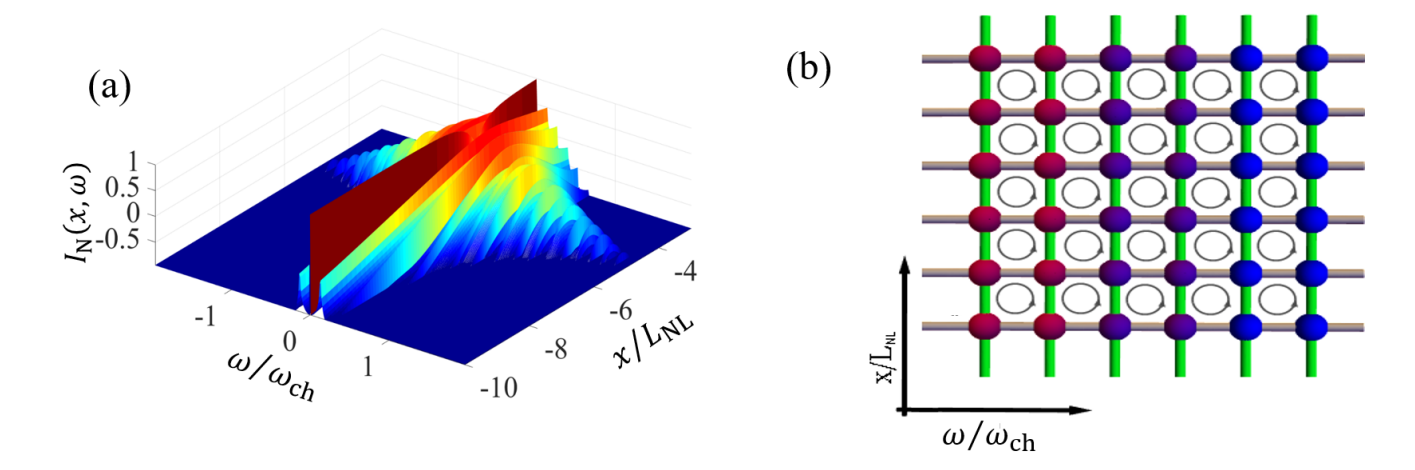


FIG. S3. Spectral dynamics of localized NSPPs through nonlinear Schrödinger equation and its corresponding synthetic lattice: panel (a) represents the evolution of spectral harmonic side-band amplitude of the SPPs for the case of Akhmediev breather excitation for a = 0.415, $P_0 = 10 \mu W$, $W \approx 3 \times 10^{-11} \text{s}^2 \cdot \text{cm}^{-1}$. Other parameters of the simulation is represented in the main text. Panel (b) of this figure also denotes the two-dimensional synthetic lattice of the excited frequency combs of NSPPs in the presence of the invariants. See the text for more details.

1. General properties

In this section we elucidate the detailed steps towards SPL formation based on excited plasmonic frequency combs and characterize the hopping in terms of nonlinear SPP field parameter. Qualitatively, the excited frequency combs within hybrid plasmonic interface are harmonic side-bands with frequency spacing Ω that act as sites of the lattice. The specific lattice sites are connected to other side-bands through characteristic hoppings (u_i) that can be characterized through correlation between amplitudes of spectral harmonic frequencies.

The characteristic lattice sites and existence of well-defined hopping justify that our frequency combs map into a synthetic frequency dimension [S32]. On the other hand, we rewrite the excited frequency combs as $A_m(\xi,\omega) := |A_m(\xi,\omega)| \exp\{i\phi_S(\xi)\}$ that are stable and can propagate up to a few nonlinear propagation length $x \approx 2L_{\rm NL}$. Specifically, we achieve invariant frequency combs for $|\omega| < \omega_{\rm ch}$ and $-5.5L_{\rm NL} < x < 4L_{\rm NL}$ as it is clearly shown in Fig. S3(a) with a well-established phase variation $\phi_S(\xi)$ but without serious amplitude distortion. Consequently, the frequency combs are spatially connected via a deterministic phase that can be achieved via Fig. 3(a) and (c). We consider this phase variation as a hopping between lattice sites in spatial space with hopping v_i .

In our analysis, we consider the π phase shift due to apparition of phase singularity and NSPP formation through Fermi-Pasta-Ulam-Tsingou recurrence [S31]. Following this assumption, we choose $N := L_{\alpha}/L_{\rm NL}$ with

$$L_{\alpha} = \frac{1}{\bar{\alpha}_{\text{eff}}}, \quad L_{\text{NL}} = \frac{1}{WP_0},$$
 (S74)

as the number of lattice sites in spatial dimension. By setting experimentally feasible parameters, the phase singularities excite for both peregrine and Akhemediev breather for $x_{\mathcal{S}} \approx L_{\alpha}/2$, $N_{\mathcal{S}} \approx N/2$. Therefore, we assume the phase pattern for spatial coordinate as

$$\phi_{\mathcal{S}} = \begin{cases} \phi_{\mathcal{NL}} & 0 < j < N_{\mathcal{S}}, \\ \pi - \phi_{\mathcal{NL}} & N_{\mathcal{S}} < j < N, \end{cases}$$
(S75)

We also use i, j dummy variables to represent the hopping along ω, x directions respectively. We define the hopping along ω axis as

$$w_{i,j} = A_i(\xi_j) A_{i+1}^*(\xi_j), \tag{S76}$$

for $A_i := A(\xi_i)$ characterize as spectral harmonic side-band amplitudes of NSPPs (see Fig. S4(a) for more details). Based on the reciprocity properties of the system we assume $A_{m,j}(\xi) = A_{-m,j}(\xi)$ and achieve the hopping for specific

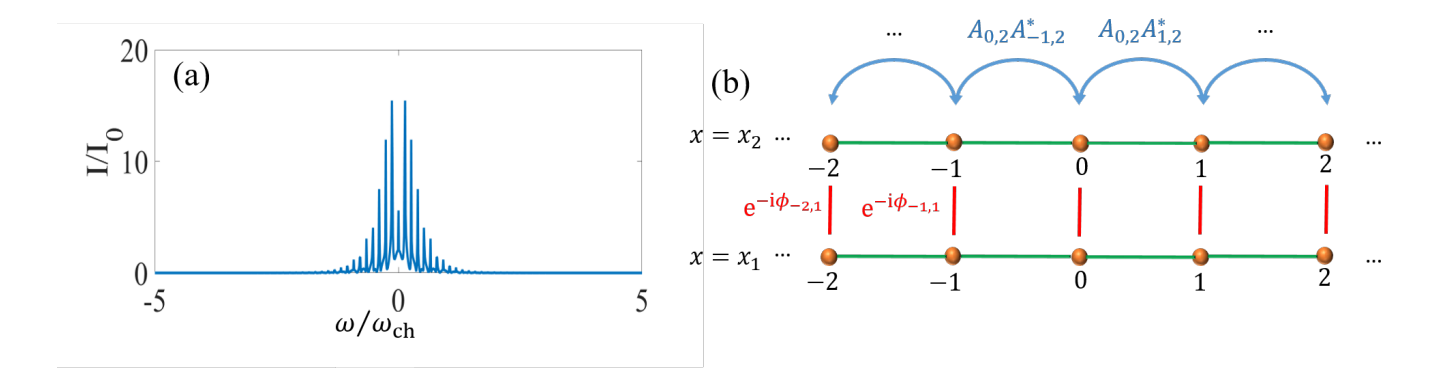


FIG. S4. Explicit mapping between the nonlinear SPP frequency combs and synthetic lattice for Akhmediev breather excitation. Panel (a) is an example of the stable propagation of nonlinear SPP field as Akhemediev breather, and panel (b) is the qualitative representation of the coupling between the different synthetic lattice. The parameter used for this simulation is the same as Fig. S3.

spatial position ξ through Eq. (S76). Moreover we assume

$$v_{i,j} := \exp\{i\varphi_{i,j}\},\tag{S77}$$

with

$$\varphi_{i,j} := \mathcal{K}(\omega_i)x - \phi_{\mathcal{S}},\tag{S78}$$

to characterize the spatial hopping for geometrical dimension, as it is clearly shown in Fig. S4(b). Consequently, we construct the synthetic lattice with well-established hopping in both spatial and spectral dimensions that can be used to investigate the dynamical evolution of the nonlinear SPP fields.

2. SPL Hamiltonian and validity of lattice description

In this section we evaluate the Hamiltonian of our synthetic lattice and achieve the dynamics of the nonlinear SPP field using this multidimensional structure. Aforementioned explanations indicate that a square lattice with two basis vector \mathbf{e}_x and \mathbf{e}_ω describes our plasmonic frequency combs. Consequently, we describe the dynamical evolution of the frequency combs within this hybrid nonlinear interface using a well-defined two-dimensional lattice with complex hopping as it is shown in Fig. S3 (b).

Then, we achieve the Hamiltonian of this synthetic lattice \mathcal{H}_{SL} as

$$\mathcal{H}_{SPL} = \sum_{i=-\mathcal{N}}^{\mathcal{N}} \sum_{j=0}^{N} \sum_{n} w_{i,j} \hat{a}_{i,j} \hat{a}_{i+n,j}^{\dagger} + \sum_{i=-\mathcal{N}}^{\mathcal{N}} \sum_{j=0}^{N} v_{i,j} \hat{a}_{i,j} \hat{a}_{i,j+1}^{\dagger} + \text{H.C.},$$
 (S79)

for n the order of coupling to other harmonic side-bands in frequency dimension. We achieve this Hamiltonian through existence the invariance of energy E, the number of excited plasmon modes \mathcal{N} and we describe the evolution of the frequency combs within this synthetic lattice through

$$|\psi(x)\rangle = \exp\{i\mathcal{H}_{\text{SPL}}x\} |\psi(x=x_0)\rangle.$$
 (S80)

In this work, we consider two kinds of NSPPs. For Akhmediev breather the spectral harmonic side-band amplitudes are obtained by Eqs. (S70), (S71), whereas for peregrine waves, we achieve the side-band by direct integration of Fourier transform or by calculating the limiting case of Akhmediev breather for $a \mapsto 0.5$.

- [S2] Y. Ma, M. Huang, S. Ryu, C. W. Bark, C. -B. Eom, P. Irvin, and J. Levy, Nano Lett. 13, 2884 (2013).
- [S3] Z. Fei, A. Rodin, G. O. Andreev, W. Bao, A. McLeod, M. Wagner, L. Zhang, Z. Zhao, M. Thiemens, G. Dominguez, et al., Nature 487, 82 (2012).
- [S4] T. Watanabe, T. Fukushima, Y. Yabe, S. A. B. Tombet, A. Satou, A. A. Dubinov, V. Y. Aleshkin, V. Mitin, V. Ryzhii, and T. Otsuji, New J. Phys. 15, 075003 (2013).
- [S5] P. Berini, Phys. Rev. B 63, 125417 (2013).
- [S6] A. Ghoshroy, Şahin K. Özdemir, and D. O. Güney, Opt. Mater. Express 10, 1862 (2020).
- [S7] D. Rodrigo, A. Tittl, O. Limaj, F. J. G. De Abajo, V. Pruneri, and H. Altug, Light: Sci. & Appl. 6, e16277 (2017).
- [S8] D. A. Steck, "Rubidium 87 d line data," (2001), https://steck.us/alkalidata/rubidium87numbers.1.6.pdf.
- [S9] Y. Zhang, Y.-W. Tan, H. L. Stormer, and P. Kim, *Nature* 438 (2005), 201.
- [S10] A. F. Page, F. Ballout, O. Hess, and J. M. Hamm, Phys. Rev. B 91, 075404 (2015).
- [S11] K. Dieckmann, R. J. C. Spreeuw, M. Weidemüller, and J. T. M. Walraven, Phys. Rev. A 58, 3891 (1998).
- [S12] S. Asgarnezhad-Zorgabad, R. Sadighi-Bonabi, and B. C. Sanders, Phys. Rev. A. 98, 013825 (2018).
- [S13] S. Asgarnezhad-Zorgabad, R. Sadighi-Bonabi, B. Kibler, Ş, K. Özdemir, and B. C. Sanders, New J. Phys. 22 (2020), 033008.
- [S14] S. Asgarnezhad-Zorgabad and B. C. Sanders, Opt. Lett. 45 (2020), 5432–5435.
- [S15] G. A. Morton, Appl. Opt. 3, 651 (1964).
- [S16] E. H. Hwang and S. Das Sarma, Phys. Rev. A 75, 205418 (2007).
- [S17] Y. V. Bludov, A. Ferreira, N. M. R. Peres, and M. I. Vasilevsky, Int. J. Mod. Phys. 27, 1341001 (2013).
- [S18] B. Wunsch, T. Stauber, F. Sols, and F. Guinea, New J. Phys. 8, 318 (2006).
- [S19] M. Jablan, H. Buljan, and M. Soljačić, Phys. Rev. B 80, 245435 (2006).
- [S20] A. Grigorenko and M. Polini and K. Novoselov, Nat. Photonics 6, 749 (2012).
- [S21] Z. Jalali-Mola and S. Jafari, J. Magn. Magn. Mater. 471, 220 (2019).
- [S22] R. E. V. Profumo, M. Polini, R. Asgari, R. Fazio, and A. H. MacDonald, Phys. Rev. B 82, 085443 (2010).
- [S23] We can derive Eq. (S23) through solving Poisson equation commensurate with boundary conditions.
- [S24] E. H. Hwang and S. Das Sarma, Phys. Rev. B 80, 205405 (2009).
- [S25] Z. Jalali-Mola and S. Jafari, Phys. Rev. B 98, 235430 (2018).
- [S26] F. Bonaccorso, Z. Sun, T. Hasan, and A. C. Ferrari, Nat. Photonics 4, 611 (2010).
- [S28] S. Asgarnezhad-Zorgabad, P. Berini, and B. C. Sanders, Phys. Rev. A 99, 051802 (2019).
- [S29] S. Asgarnezhad-Zorgabad, Sci. Rep. 11, 3450 (2021).
- [S30] B. Kibler, J. Fatome, C. Finot, G. Millot, F. Dias, G. Genty, N. Akhmediev, and J. M. Dudley, Nat. Phys. 6, 790 (2010).
- [S31] D. Pierangeli, M. Flammini, L. Zhang, G. Marcucci, A. J.Agranat, P. G. Grinevich, P. M. Santini, C. Conti, and E. Del Re, Phys. Rev. X 8, 041017 (2018).
- [S32] L. Yuan, Q. Lin, M. Xiao, and S. Fan, Optica 5, 1396 (2018).
- [S33] Y. Lai and H. A. Haus, Phys. Rev. A 40, 844 (1989).